PandaX-II constraints on spin-dependent WIMP-nucleon effective interactions

Jingkai Xia [a], Abdusalam Abdukerim [b], Wei Chen [a], Xun Chen [a], Yunhua Chen [c], Xiangyi Cui [a], Deqing Fang [d], Changbo Fu [a], Karl Giboni [a], Franco Giuliani [a], Linhui Gu [a], Xuyuan Guo [c], Zhifan Guo [e], Ke Han [a], Changda He [a], Shengming He [c], Di Huang [a], Xingtao Huang [f], Zhou Huang [a], Peng Ji [g], Xiangdong Ji [a,h,1], Yonglin Ju [e], Shaoli Li [a], Heng Lin [a], Huaxuan Liu [e], Jianglai Liu [a,h], Yugang Ma [d], Yajun Mao [i], Kaixiang Ni [a], Jinhua Ning [c], Xiangxiang Ren [a], Fang Shi [a], Andi Tan [j], Anqing Wang [f], Cheng Wang [e], Hongwei Wang [d], Meng Wang [f], Qiuhong Wang [d], Siguang Wang [i], Xiuli Wang [e], Xuming Wang [a], Zhou Wang [e], Mengmeng Wu [g], Shiyong Wu [c], Mengjiao Xiao [j,k], Pengwei Xie [h], Binbin Yan [f], Jijun Yang [a], Yong Yang [a], Chunxu Yu [g], Jumin Yuan [f], Jianfeng Yue [c], Dan Zhang [j], Hongguang Zhang [a], Tao Zhang [a], Li Zhao [a], Qibin Zheng [l], Jifang Zhou [c], Ning Zhou [a,*], Xiaopeng Zhou [i], Wick C. Haxton [m,n,**]

[a] School of Physics and Astronomy, Shanghai Jiao Tong University, Shanghai Key Laboratory for Particle Physics and Cosmology, Shanghai 200240, China
[b] School of Physics and Technology, Xinjiang University, Ürümqi 830046, China
[c] Yalong River Hydropower Development Company, Ltd., 288 Shuanglin Road, Chengdu 610051, China
[d] Shanghai Institute of Applied Physics, Chinese Academy of Sciences, Shanghai 201800, China
[e] School of Mechanical Engineering, Shanghai Jiao Tong University, Shanghai 200240, China
[f] School of Physics and Key Laboratory of Particle Physics and Particle Irradiation (MOE), Shandong University, Jinan 250100, China
[g] School of Physics, Nankai University, Tianjin 300071, China
[h] Tsung-Dao Lee Institute, Shanghai 200240, China
[i] School of Physics, Peking University, Beijing 100871, China
[j] Department of Physics, University of Maryland, College Park, MD 20742, USA
[k] Center of High Energy Physics, Peking University, Beijing 100871, China
[l] School of Medical Instrument and Food Engineering, University of Shanghai for Science and Technology, Shanghai 200093, China
[m] Department of Physics, University of California, Berkeley, CA 94720, USA
[n] Lawrence Berkeley National Laboratory, Berkeley, CA 94720, USA

ARTICLE INFO

ABSTRACT

We present PandaX-II constraints on candidate WIMP-nucleon effective interactions involving the nucleon or WIMP spin, including, in addition to standard axial spin-dependent (SD) scattering, various couplings among vector and axial currents, magnetic and electric dipole moments, and tensor interactions. The data set corresponding to a total exposure of 54-ton-days is reanalyzed to determine constraints as a function of the WIMP mass and isospin coupling. We obtain WIMP-nucleon cross section bounds of 1.6×10^{-41} cm^2 and 9.0×10^{-42} cm^2 (90% c.l.) for neutron-only SD and tensor coupling, respectively, for a mass $M_{\mathrm{WIMP}} \sim 40$ GeV/c^2. The SD limits are the best currently available for $M_{\mathrm{WIMP}} > 40$ GeV/c^2. We show that PandaX-II has reached a sensitivity sufficient to probe a variety of other candidate spin-dependent interactions at the weak scale.

* Corresponding author at: School of Physics and Astronomy, Shanghai Jiao Tong University, Shanghai, 200240, China.
** Corresponding author at: Department of Physics, University of California, Berkeley, CA 94720, USA.
E-mail addresses: xdji@sjtu.edu.cn (X. Ji), nzhou@sjtu.edu.cn (N. Zhou), haxton@berkeley.edu (W.C. Haxton).
1 Spokesperson of PandaX Collaboration.

Astrophysical and cosmological observations indicate that a large amount of non-luminous dark matter (DM) exists in our universe, constituting $\sim 27\%$ of the closure density. However, the exact nature of DM remains a mystery. One intriguing DM candidate, a weakly-interacting massive particle (WIMP), arises naturally in many extensions of the standard model [1,2]. Many WIMP searches have been performed, including direct detection of their scattering off target nuclei, indirect detection of their decay or annihilation, and their production in collider experiments. In the analysis of direct detection experiments, frequently it is assumed that the scattering arises from the light-quark-level (u, s, d) effective interaction

$$\mathcal{L} \sim \frac{G_F}{\sqrt{2}} \sum_q \left[\bar{\chi} \gamma_\mu \chi \, c_q^{VV} \bar{q} \gamma^\mu q + \bar{\chi} \gamma_\mu \gamma_5 \chi \, c_q^{AA} \bar{q} \gamma^\mu \gamma_5 q \right] \qquad (1)$$

which can be reduced to a nucleon-level operator useful in analyzing the nuclear response to WIMP scattering [3]. Limits on the vector spin-independent (SI) and axial spin-dependent (SD) WIMP-proton and WIMP-neutron cross sections $\sigma_{p,n}^{\mathrm{SI,SD}}$ can then be derived. The recent stringent direct detection null results obtained successively by LUX [4,5], PandaX [6,7] and XENON [8–10] have significantly tighten the bounds on $\sigma_{p,n}^{\mathrm{SI,SD}}$ [11].

The interaction of Eq. (1) was motivated by supersymmetric DM candidates, like the neutralino, that can naturally account for the DM relic density. The motivation to focus exclusively on such candidates has weakened due in particular to collider constraints [12]. An alternative approach, effective field theory (EFT) [13–15], has gained favor because it allows one to do an analysis [16–19] free of theory assumptions. One selects an EFT scale – e.g., the light-quark or a nucleon scale – and constructs a complete basis of effective operators to a given order, taking into account all general symmetries limiting that basis. The underlying UV theory of DM will reduce at that scale to some definite combination of the basis operators, regardless of its nature. Experimentalists can explore the sensitivities of their detectors to the basis operators, to make sure they are probing all possibilities. The EFT approach has shown 1) relative experimental sensitivities depend on the operator choice, and 2) direct detection is potentially more powerful than might appear from SI/SD analyses, as six (not two) independent constraints on DM can be obtained, in principle [15].

The PandaX-II detector, located in the China Jinping Underground Laboratory (CJPL), is a dual-phase xenon time-projection chamber with 580 kg of liquid xenon in the sensitive target volume. When the incoming WIMP scatters off a xenon nucleus, both the prompt scintillation photons (S1) in the liquid and the delayed proportional scintillation photons (S2) in the gas are collected by 55 top and 55 bottom Hamamatsu R11410-20 3-inch photomultiplier tubes. The experiment has an accumulated exposure of 54-ton-days [6]. The previously reported analysis for the standard (isoscalar) SI interaction yielded a 90% exclusion limit on σ^{SI} of 8.6×10^{-47} cm^2 for a WIMP mass of 40 GeV/c^2. (These bounds were recently superseded by XENON1T results [10].) In this paper we present PandaX-II constraints a variety of candidate interactions that depend on nucleon or WIMP spin.

Spin-dependent interactions other than SD can arise from WIMP magnetic and electric dipole moments, vector-axial interference terms, tensor interactions, etc. While the associated nucleon-level effective operators are conventionally expressed in covariant form, they can be rewritten in terms of the Galilean-invariant EFT basis used here, convenient for nonrelativistic shell model (SM) treatments of the nuclear physics. This basis consists of fourteen operators generated at next-to-next-to-leading-order from the nucleon-WIMP perpendicular relative velocity operator $\vec{v}^\perp$, the momentum transfer $\vec{q}$, and the WIMP and nucleon spins, $\vec{S}_\chi$ and $\vec{S}_N$ [15].

We specialize to the scattering of a spin-1/2 WIMPs off a natural xenon target, exploring four dimension-four and three higher dimension effective interactions, selected from Table 1 of Ref. [15]. The operator dimension is defined as $4 +$ number of powers of m_M in the denominator, where m_M is a scale that governs the strength of the WIMP and nucleon moments being coupled. The dimension-four operators are the V-A interactions

$$
\begin{aligned}
\mathcal{L}_{\mathrm{int}}^5 &\equiv \bar{\chi} \gamma^\mu \chi \, \bar{N} \gamma_\mu N \to \mathcal{O}_1 \\
\mathcal{L}_{\mathrm{int}}^7 &\equiv \bar{\chi} \gamma^\mu \chi \, \bar{N} \gamma_\mu \gamma^5 N \to -2\mathcal{O}_7 + 2\frac{m_N}{m_\chi} \mathcal{O}_9 \\
\mathcal{L}_{\mathrm{int}}^{13} &\equiv \bar{\chi} \gamma^\mu \gamma^5 \chi \, \bar{N} \gamma_\mu N \to 2\mathcal{O}_8 + 2\mathcal{O}_9 \\
\mathcal{L}_{\mathrm{int}}^{15} &\equiv \bar{\chi} \gamma^\mu \gamma^5 \chi \, \bar{N} \gamma_\mu \gamma^5 N \to -4\mathcal{O}_4
\end{aligned} \qquad (2)
$$

with m_N the nucleon mass and $\mathcal{O}_1 = 1_\chi 1_N$, $\mathcal{O}_4 = \vec{S}_\chi \cdot \vec{S}_N$, $\mathcal{O}_7 = \vec{S}_N \cdot \vec{v}^\perp$, $\mathcal{O}_8 = \vec{S}_\chi \cdot \vec{v}^\perp$, and $\mathcal{O}_9 = i(\vec{S}_\chi \times \vec{S}_N) \cdot \frac{\vec{q}}{m_N}$ the nonrelativistic operators of [14,15]. While $\mathcal{L}_{\mathrm{int}}^5$ generates the standard SI interaction, the other interactions involve an axial coupling and thus depend on spin.

One can equally well start with a basis of light-quark effective operators, reducing these via chiral EFT to their nonrelativistic nucleon equivalents [20,21]. The spin-dependent nucleon-level operators arising from the axial part of Eq. (1) (the standard SD interaction) and from the light-quark tensor interaction will be considered here.

The dimension-five operators coupling the WIMP magnetic or electric dipole moments with the nucleon's vector current, and the dimension-six operator coupling WIMP and nucleon magnetic moments, are examples of other potential sources of spin-dependent scattering,

$$
\begin{aligned}
\mathcal{L}_{\mathrm{int}}^9 &\equiv \bar{\chi} i \sigma^{\mu\nu} \frac{q_\nu}{m_M} \chi \, \bar{N} \gamma_\mu N \\
&\to -\frac{\vec{q}^{\,2}}{2 m_\chi m_M} \mathcal{O}_1 + \frac{2 m_N}{m_M} \mathcal{O}_5 - \frac{2 m_N}{m_M}(\frac{\vec{q}^{\,2}}{m_N^2} \mathcal{O}_4 - \mathcal{O}_6) \\
\mathcal{L}_{\mathrm{int}}^{17} &\equiv i \bar{\chi} i \sigma^{\mu\nu} \frac{q_\nu}{m_M} \gamma^5 \chi \, \bar{N} \gamma_\mu N \to \frac{2 m_N}{m_M} \mathcal{O}_{11} \\
\mathcal{L}_{\mathrm{int}}^{10} &\equiv \bar{\chi} i \sigma^{\mu\nu} \frac{q_\nu}{m_M} \chi \, \bar{N} i \sigma_{\mu\alpha} \frac{q^\alpha}{m_M} N \to 4(\frac{\vec{q}^{\,2}}{m_M^2} \mathcal{O}_4 - \frac{m_N^2}{m_M^2} \mathcal{O}_6)
\end{aligned} \qquad (3)
$$

Here $\mathcal{O}_5 = i\vec{S}_\chi \cdot (\frac{\vec{q}}{m_N} \times \vec{v}^\perp)$, $\mathcal{O}_6 = (\vec{S}_\chi \cdot \frac{\vec{q}}{m_N})(\vec{S}_N \cdot \frac{\vec{q}}{m_N})$, and $\mathcal{O}_{11} = i\vec{S}_\chi \cdot \frac{\vec{q}}{m_N}$. The dependence on $\vec{q}$ implies nuclear form factors that peak at larger momentum transfers, influencing experimental strategies for optimally constraining such interactions. We set $m_M \equiv m_N$, normalizing both WIMP and nucleon moments to the nucleon scale.

Each operator $\mathcal{L}_{\mathrm{int}}^i$ can have independent couplings to protons and neutrons, or equivalently to isospin [15],

$$\frac{d_i^0}{m_V^2} + \frac{d_i^1}{m_V^2} \tau_3 = \frac{d_i^p}{m_V^2} \frac{1 + \tau_3}{2} + \frac{d_i^n}{m_V^2} \frac{1 - \tau_3}{2} \qquad (4)$$

where τ_3 is the Pauli isospin operator. The couplings d_i are dimensionless, defined relative to the weak scale

$$m_V \equiv \langle v \rangle = (2 G_F)^{-\frac{1}{2}} = 246.2 \text{ GeV}$$

with $\langle v \rangle$ the Higgs vacuum expectation value. We will consider isoscalar ($d_i^1 = 0$) and isovector ($d_i^0 = 0$) interactions, for which $d_i^p = d_i^n$ and $-d_i^p = d_i^n$, respectively; as well as couplings only to protons ($d_i^1 = d_i^0$) or neutrons ($d_i^1 = -d_i^0$). For our higher-dimension operators, the d_i's also encode information about the

absolute size of the WIMP electric and dipole moments, given that we have normalized to nucleonic values ($m_M \equiv m_N$).

As the spin response of Xe is largely governed by the unpaired neutrons in ^{129,131}Xe, one expects the $1 - \tau_3$ projection of nucleon-spin operators to dominate.

The differential cross section for elastic scattering is

$$\frac{d\sigma(v, E_R)}{dE_R} = 2m_T \frac{d\sigma(v, \vec{q}^{\,2})}{d\vec{q}^{\,2}}$$

$$= \frac{2m_T}{4\pi v^2} \left[\frac{1}{2J_\chi + 1} \frac{1}{2J + 1} \sum_{\text{spins}} |\mathcal{M}|^2 \right] \quad (5)$$

where the square of the Galilean invariant amplitude $\mathcal{M}$ is a product of WIMP and nuclear matrix elements and is a function of initial WIMP velocity v (dimensionless, in units of c) and the three-momentum transfer $\vec{q}$ [15]. Here J_χ is the WIMP spin and J the nuclear ground state angular momentum. In the long wavelength limit the nuclear response functions corresponding to matrix elements of simple operators familiar from weak interactions, such as $1(i)$, $\vec{\sigma}(i)$, $\vec{\ell}(i)$, and $\vec{\sigma}(i) \cdot \vec{\ell}(i)$. The differential event rate with respect to nuclear recoil energy is

$$\frac{dR}{dE_R} = \frac{\rho_\chi}{m_\chi} \int \frac{d\sigma(v, E_R)}{dE_R} v f(\vec{v}) d^3 v, \quad (6)$$

where the $f(\vec{v})$ is the normalized velocity distribution of the WIMP particles. We calculate WIMP signal rates by evaluating Eq. (6) for a local WIMP mass density of $\rho_\chi = 0.3$ GeV/c^2/cm^3, assuming a Maxwellian WIMP velocity distribution peaked at $v_0 = 220$ km/s and truncated at the galactic escape velocity $v_{esc} = 544$ km/s.

The nuclear response functions for DM elastic scattering must be calculated before experimental limits can be converted to bounds on the operator coefficients of Eq. (4). For each contributing Xe isotope and needed operator, we performed full-basis shell-model calculations using the GCN5082 [22] interaction (so named because the SM valence space resides between the shell closures at nucleon numbers 50 and 82). The calculations were done without truncation, using the SM code BIGSTICK to treat bases that ranged to 9 billion Slater determinants [23]. Full GCN5082 Xe isotopes response functions are used in the Mathematica script of [24], an update of [15]. This script and the associated library of one-body nuclear density matrices are available on request from the authors of [24]. The scripts of [24] and [15] were carefully cross-checked against one another, to verify their consistency.

Fig. 1 shows computed recoil energy spectra. The upper panels include the coherent isoscalar (N+Z) and isovector (N-Z) SI responses (operator $\mathcal{L}_{int}^5$), which we show for normalization. Though we used SM results, simple phenomenological forms [25] also work well, below the diffraction minimum, as the form factor is governed by its known $q = 0$ value and the nuclear radius.

The remaining curves corresponding to interactions with nucleon spin ($\mathcal{L}_{int}^7$), WIMP spin ($\mathcal{L}_{int}^{13}$), or both ($\mathcal{L}_{int}^{15}$), at two WIMP masses. All curves correspond to weak-scale interactions: with $d_i^p = d_i^n \equiv 1$ ($d_i^p = -d_i^n \equiv 1$) for isoscalar (isovector) coupling. The lower panels show the corresponding results for the magnetic and electric dipole moment interactions, $\mathcal{L}_{int}^9$, $\mathcal{L}_{int}^{10}$, and $\mathcal{L}_{int}^{17}$.

The WIMP couplings d_i are constrained by PandaX-II rate limits. We use data from two low-background physics runs with a total exposure of 54-ton-days, Run 9 with 79.6 live days in 2016 and Run 10 with 77.1 live days in 2017. Calibration data from an AmBe source outside the cryogenic vessel and tritium decays from CH$_3$T injected into the Xe provided tests of the detector response to the nuclear (NR) and electron (ER) recoil events, respectively [6]. A
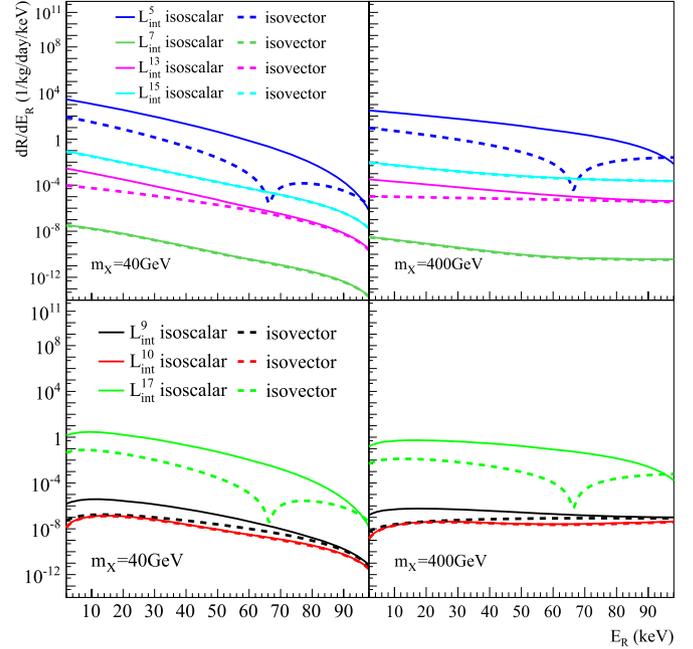

Fig. 1. Recoil energy spectra for the scattering of spin-$\frac{1}{2}$ WIMPs on xenon nuclei, for WIMP masses of 40 GeV/c^2 and 400 GeV/c^2, and unit isoscalar ($d_i^0 = 1$, $d_i^1 = 0$) and isovector ($d_i^0 = 0$, $d_i^1 = 1$) coupling. Top panel: dimension-four V-A interactions. Bottom panel: higher dimension magnetic and electric dipole interactions.

NEST-based Monte Carlo (MC) simulation (Ref. [26] for ER, Ref. [27] for NR) of the data in the (S1, S2) distribution is optimized by adjusting the initial excitation-to-ionization ratio and the recombination fluctuation. A reliable tuned NEST model for PandaX-II is obtained for S1 up to 50 photoelectrons (PEs). The S1 and S2 signal distributions for a given EFT interaction are simulated using the tuned NEST model and PandaX-II detector response parameters [6].

Our event selection criteria follow Ref. [6]: S1 from 3 to 45 PEs, S2 from 100 (raw, not corrected for electron lifetime) to 10000 PEs, events lying within the 99.99% NR acceptance, and the total fiducial target of 329 ± 16 kg. The backgrounds in Run 9 and Run 10, estimated in Ref. [6], are dominated by ^{127}Xe, tritium, other flat ER background (^{85}Kr, radon and detector gamma background), accidental, and neutron contributions.

This search window can include nuclear recoil event energies up to 100 keV$_{nr}$ (NR energy) due to the smearing of S1 and S2, although the efficiency drops below 50% above 35 keV$_{nr}$ on average. For dimension-four operators, the majority of signal events have nuclear recoil energy below 35 keV$_{nr}$. The overall signal selection efficiency is between 40% and 50%, very similar to that for the SI analysis in Ref. [6]. For dimension-five or dimension-six operators, the analysis is more complicated due to the sharper form factor momentum dependence. For instance, the signal efficiency for the isovector $\mathcal{L}_{int}^9$ operator decreases from 65% to 6.5% as the WIMP mass increases from 40 to 400 GeV. Thus efficiencies can be improved by adjusting search windows according to operator type and WIMP mass, as LUX has described [28]. Such strategies will be explored in future PandaX analyses: detector calibration studies for S1 above 50 PE will be needed to implement such window adjustments.

We constrain the WIMP-nucleon EFT couplings d_i as a function of the WIMP mass, following the likelihood analysis of Ref. [6]. A standard profile likelihood test statistic was determined as a function of WIMP mass and cross section, and compared with that from a large number of toy MC calculations to derive the upper limits of the signal yields at 90% confidence level (C.L.) [29,30].
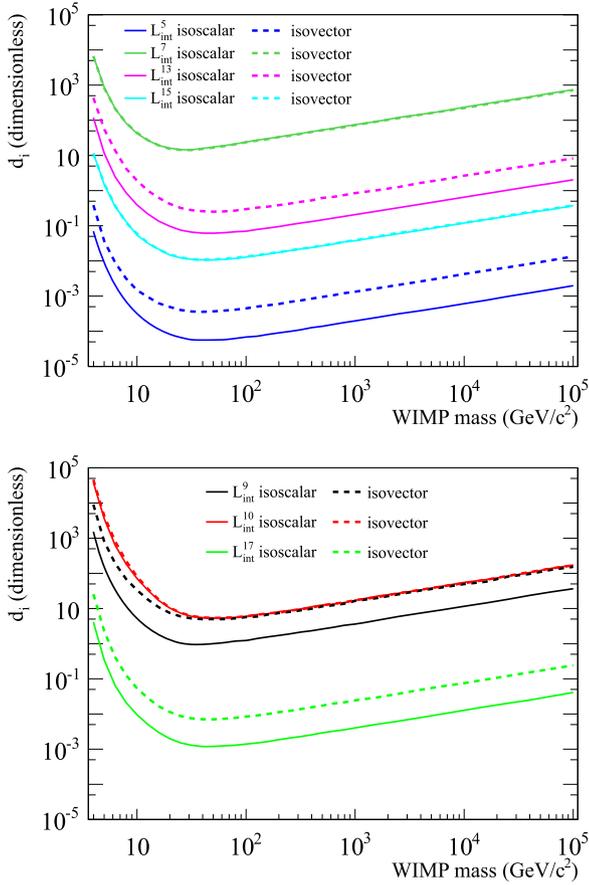
Fig. 2. Exclusion limits on the coefficients of dimension-four (top panel) and higher dimension (bottom panel) operators.

Fig. 3. Recoil energy spectra for the scattering of spin-$\frac{1}{2}$ WIMPs on xenon nuclei, for WIMP masses of 40 GeV/c^2 and 400 GeV/c^2, for SD and tensor interactions. The top (bottom) panel corresponds to neutron-only (proton-only) coupling.

The upper panel of Fig. 2 gives PandaX-II bounds on the coherent SI interaction $\mathcal{L}_{\text{int}}^5$ as well as the spin-spin interaction $\mathcal{L}_{\text{int}}^{15}$, related to the traditional SD interaction discussed below. They are well below the nominal weak scale $d \sim 1$ over all or almost all WIMP mass range illustrated. The isoscalar coupling limit $|d_5^0| < 5.6 \cdot 10^{-5}$ at maximum sensitivity (~ 40 GeV WIMP) corresponds to the PandaX-II cross section bound $\sigma_{p,n}^{\text{SI}} < 8.6 \cdot 10^{-47}$ cm^2. But limits on the axial (WIMP) – vector (nucleus) coupling $d_{13}^{0,1}$ are also at the weak scale, illustrating the power of current-generation experiments to probe momentum- or velocity-dependent interactions. The lower panel gives the corresponding bounds for interaction involving WIMP magnetic and electric dipole moments. The bounds are near and in one case (the WIMP electric dipole moment coupling to the nucleon vector current $\mathcal{L}_{\text{int}}^{17}$) below the nominal weak scale. Bounds given in the lower panel also include an implicit dimensionless factor representing any needed rescaling of the WIMP moments to their physical values, relative to the nucleon scale we adopted via $m_M \sim m_N$.

An often-used measure of experimental sensitivity to spin-dependent WIMP scattering is provided by the SD axial nucleon-level operator obtained from Eq. (1),

$$\mathcal{O}_{\text{SD}} \equiv \frac{g_A(q^2)}{g_A(0)} \mathcal{O}_4 - \frac{m_N g_P(q^2)}{2 g_A(0)} \mathcal{O}_6 \qquad (7)$$

with the specific combination of nucleon-level axial and induced pseudoscalar operators dependent on isospin through the C_q^{AA}. The pseudoscalar coupling is enhanced in the isovector channel by pion-pole dominance. Comparisons are typically made by selecting
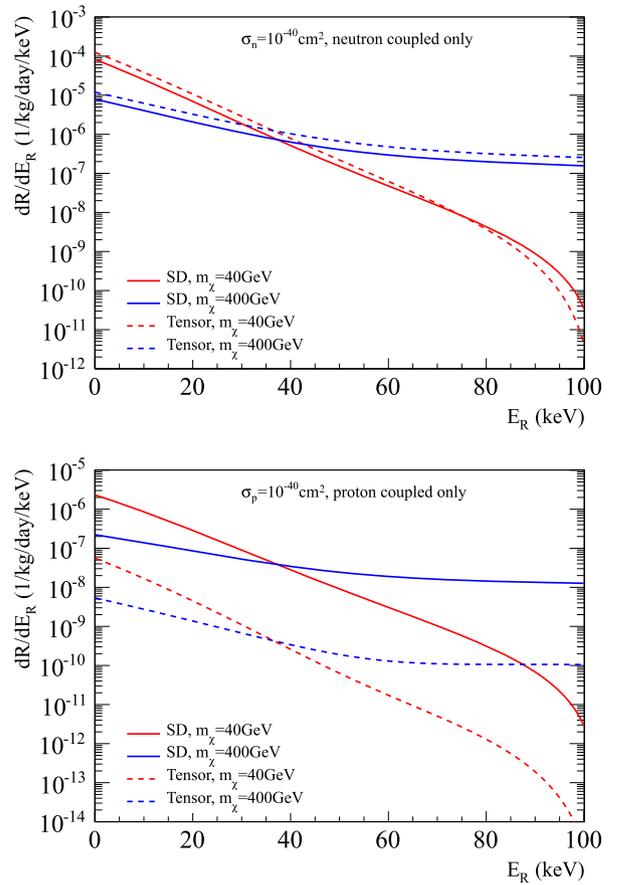
proton-only (p) or neutron-only (n) couplings. The nuclear cross section $\sigma_{p,n}^{\text{SD}\,A}$ is related to the nucleon cross section $\sigma_{p,n}^{\text{SD}}$ by

$$\sigma_{p,n}^{\text{SD}\,A}(q^2) = \frac{4\pi}{3(2J+1)} \left(\frac{\mu_A}{\mu_{p,n}} \right)^2 S_{p,n}^A(q^2) \sigma_{p,n}^{\text{SD}} \qquad (8)$$

where μ_A ($\mu_{p,n}$) is the reduced mass for scattering off the nucleus (nucleon), and $S_{p,n}^A(q^2)$ is the nuclear spin structure function that we take from [3], including exchange current corrections. Fig. 3 shows recoil spectra for the SD and tensor cross sections.

The 90% C.L. cross section limits are shown in Fig. 4. The optimal bounds, obtained at $M_{\text{WIMP}} \sim 40$ GeV/c^2, limit σ_n^{SD} (neutron-only) and σ_p^{SD} (proton-only) to 1.6×10^{-41} cm^2 and 4.4×10^{-40} cm^2, respectively. The results modestly improve existing LUX bounds [4] for $M_{\text{WIMP}} > 40$ GeV/c^2.

Models of asymmetric dark matter favor Dirac fermion WIMPs, where candidate dimension-4 effective operators include the SD and tensor $\bar{\chi}\sigma_{\mu\nu}\chi \; \bar{q}\sigma^{\mu\nu}q$ operators. Constraints from direct detection are particularly competitive for the latter [38]. The tensor interaction generates, after a leading-order chiral reduction [21], the nucleon-level operator $8\mathcal{O}_4$. The dashed curve in the top panel of Fig. 4 shows the neutron-only PandaX-II limits. Bounds on σ_n^{T} and σ_p^{T} of 9.0×10^{-42} cm^2 and 2.2×10^{-38} cm^2, respectively, are found at $M_{\text{WIMP}} \sim 40$ GeV.

In conclusion, we have presented new limits on a candidate spin-dependent WIMP interactions, using PandaX-II Run 9 and Run 10 data with an exposure of 54-ton-days. In addition to the standard SD interaction, we considered vector-axial vector interferences, interactions generated by WIMP magnetic and
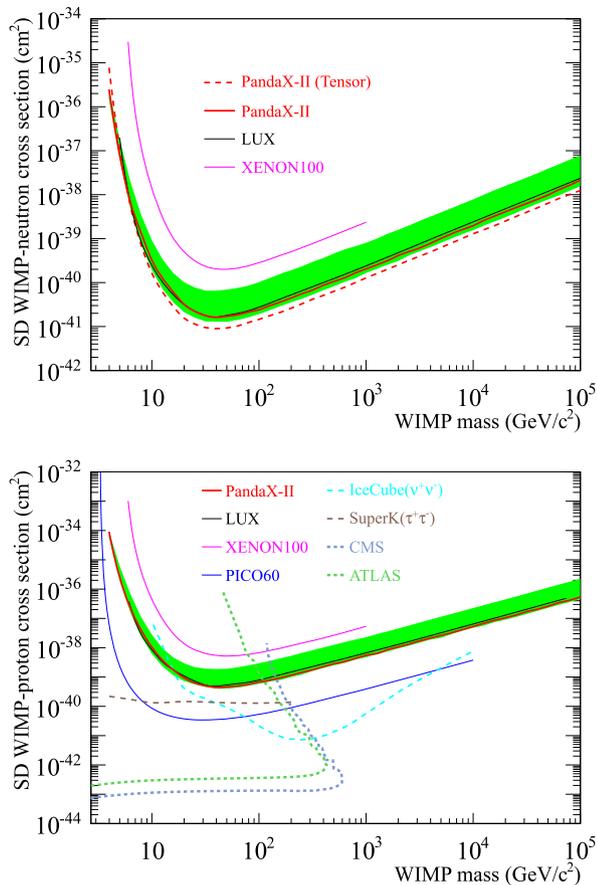
Fig. 4. PandaX-II exclusion limits on the WIMP-nucleon cross section for the standard SD interaction assuming neutron-only (top panel) and proton-only (bottom panel) coupling. The 1σ sensitivity bands are shown in green. Also shown are recent results from LUX [5], XENON100 [9], ATLAS [31], CMS [32], PICO-2L [33], PICO-60 [34,35], IceCube [36] and Super-K [37]. The dashed line (top panel) gives PandaX-II limits on tensor WIMP-neutron couplings.

electric dipole moments, and tensor interactions. We showed that PandaX-II has achieved sufficient sensitivity to probe certain velocity- and momentum-dependent interactions at the weak scale. We obtained the most stringent upper limits to date on σ_n^{SD} for M_{WIMP} above 40 GeV/c^2, with a lowest excluded value of 1.6×10^{-41}cm^2 at 40 GeV/c^2, 90% c.l. The corresponding proton and tensor interaction constraints are $\sigma_p^{SD} < 4.4 \times 10^{-40}$ cm^2, $\sigma_n^T < 9.0 \times 10^{-42}$ cm^2, and $\sigma_p^T < 2.2 \times 10^{-38}$ cm^2.

ful discussions on the EFT models in direct detection experiment. Finally, we thank the CJPL administration and the Yalong River Hydropower Development Company Ltd. for indispensable logistical support and other help.

References

[1] J.L. Feng, Dark matter candidates from particle physics and methods of detection, Annu. Rev. Astron. Astrophys. 48 (2010) 495–545, https://doi.org/10.1146/annurev-astro-0082708-101659.

[2] G. Bertone, D. Hooper, J. Silk, Particle dark matter: evidence, candidates and constraints, Phys. Rep. 405 (2005) 279, https://doi.org/10.1016/j.physrep.2004.08.031.

[3] P. Klos, J. Menendez, D. Gazit, A. Schwenk, Large-scale nuclear structure calculations for spin-dependent WIMP scattering with chiral effective field theory currents, Phys. Rev. D 88 (2013) 083516, https://doi.org/10.1103/PhysRevD.88.083516;
See also J. Engel, S. Pittel, P. Vogel, Int. J. Mod. Phys. E 1 (1992) 1.

[4] D. Akerib, et al., Results from a search for dark matter in the complete LUX exposure, Phys. Rev. Lett. 118 (2017) 021303, https://doi.org/10.1103/PhysRevLett.118.021303.

[5] D.S. Akerib, et al., Limits on spin-dependent WIMP-nucleon cross section obtained from the complete LUX exposure, Phys. Rev. Lett. 118 (2017) 251302, https://doi.org/10.1103/PhysRevLett.118.251302.

[6] X. Cui, et al., Dark matter results from 54-ton-day exposure of PandaX-II experiment, Phys. Rev. Lett. 119 (2017) 181302, https://doi.org/10.1103/PhysRevLett.119.181302.

[7] C. Fu, et al., Spin-dependent weakly-interacting-massive-particle–nucleon cross section limits from first data of PandaX-II experiment, Phys. Rev. Lett. 118 (2017) 071301, https://doi.org/10.1103/PhysRevLett.118.071301.

[8] E. Aprile, et al., First dark matter search results from the XENON1T experiment, Phys. Rev. Lett. 119 (2017) 181301, https://doi.org/10.1103/PhysRevLett.119.181301.

[9] E. Aprile, et al., XENON100 dark matter results from a combination of 477 live days, Phys. Rev. D 94 (2016) 122001, https://doi.org/10.1103/PhysRevD.94.122001.

[10] E. Aprile, et al., Dark matter search results from a one tonne×year exposure of XENON1T, Phys. Rev. Lett. 121 (2018) 111302, https://doi.org/10.1103/PhysRevLett.121.111302.

[11] J. Liu, X. Chen, X. Ji, Current status of direct dark matter detection experiments, Nat. Phys. 13 (2017) 212, https://doi.org/10.1038/NPHYS4039.

[12] M.E. Peskin, Supersymmetric dark matter in the harsh light of the large hadron collider, Proc. Natl. Acad. Sci. USA 112 (2015) 12256.

[13] J. Fan, M. Reece, L.-T. Wang, Non-relativistic effective theory of dark matter direct detection, J. Cosmol. Astropart. Phys. 1011 (2010) 042, https://doi.org/10.1088/1475-7516/2010/11/042.

[14] A.L. Fitzpatrick, W.C. Haxton, E. Katz, N. Lubbers, Y. Xu, The effective theory of dark matter detection, J. Cosmol. Astropart. Phys. 02 (2013) 004.

[15] N. Anand, A.L. Fitzpatrick, W.C. Haxton, Weakly interacting massive particle-nucleus elastic scattering response, Phys. Rev. C 89 (2014) 065501, https://doi.org/10.1103/PhysRevC.89.065501.

[16] K. Schneck, et al., Dark matter effective field theory scattering in direct detection experiments, Phys. Rev. D 91 (2015) 092004, https://doi.org/10.1103/PhysRevD.91.092004.

[17] E. Aprile, et al., Effective field theory search for high-energy nuclear recoils using the XENON100 dark matter detector, Phys. Rev. D 96 (2017) 042004, https://doi.org/10.1103/PhysRevD.96.042004.

[18] Z. Liu, Y. Su, Y.S. Tsai, B. Yu, Q. Yuan, A combined analysis of PandaX, LUX and XENON1T experiments within the framework of dark matter effective theory, J. High Energy Phys. 11 (2017) 024, https://doi.org/10.1007/JHEP11(2017)024.

[19] S. Kang, S. Scopel, G. Tomar, J.-H. Yoon, Present and projected sensitivities of dark matter direct detection experiments to effective WIMP-nucleus couplings, arXiv:1805.06113.

[20] M. Hoeferichter, P. Klos, A. Schwenk, Chiral power counting of one- and two-body currents in direct detection of dark matter, Phys. Lett. B 746 (2015) 410.

[21] F. Bishara, J. Brod, B. Grinstein, J. Zupan, From quarks to nucleons in dark matter direct detection, J. High Energy Phys. 1711 (2017) 059.

[22] J. Menendez, A. Poves, E. Caurier, F. Nowacki, Disassembling the nuclear matrix elements of the neutrinoless $\beta\beta$ decay, Nucl. Phys. A 818 (2009) 139, https://doi.org/10.1016/j.nuclphysa.2008.12.005;
See also L. Vietze, et al., Phys. Rev. D 91 (2015) 043520 for a comparison of GCN5082 Xe isotope spectroscopic predictions to experiment and for full-space calculations of certain isotopes (^{132}Xe, ^{134}Xe, ^{136}Xe) that provide valuable numerical cross checks on present work; in other cases Vietze et al. had to make truncations, which are avoided in the present work.

[23] C.W. Johnson, Current status of very-large-basis Hamiltonian diagonalizations for nuclear physics, arXiv:1809.07869, to be published in the Proc. of CIPANP18;
C.W. Johnson, et al., arXiv:1801.08432.

[24] A.L. Fitzpatrick, W.C. Haxton, C. Johnson, K.S. McElvain, Annu. Rev. Nucl. Part. Sci. (2019), in preparation.

[25] J.D. Lewin, P.F. Smith, Review of mathematics, numerical factors, and corrections for dark matter experiments based on elastic nuclear recoil, Astropart. Phys. 6 (1996) 87, https://doi.org/10.1016/S0927-6505(96)00047-3.

[26] M. Szydagis, A. Fyhrie, D. Thorngren, M. Tripathi, Enhancement of NEST capabilities for simulating low-energy recoils in liquid xenon, J. Instrum. 8 (2013) C10003, https://doi.org/10.1088/1748-0221/8/10/C10003.

[27] B. Lenardo, K. Kazkaz, A. Manalaysay, J. Mock, M. Szydagis, M. Tripathi, A global analysis of light and charge yields in liquid xenon, IEEE Trans. Nucl. Sci. 62 (2015) 3387, https://doi.org/10.1109/TNS.2015.2481322.

[28] N. Larsen, the LUX Collaboration, LUX sensitivity to effective field theory interactions, in: Proceedings of CIPANP18, CIPANP18, 2018, to be published by SLAC eConf, https://conferences.lbl.gov/event/137/session/19/contribution/271.

[29] A.L. Read, Presentation of search results: the cl_s technique, J. Phys. G 28 (2002) 2693, https://doi.org/10.1088/0954-3899/28/10/313.

[30] T. Junk, Confidence level computation for combining searches with small statistics, Nucl. Instrum. Methods Phys. Res., Sect. A, Accel. Spectrom. Detect. Assoc. Equip. 434 (1999) 435, https://doi.org/10.1016/S0168-9002(99)00498-2.

[31] M. Aabound, et al., Search for dark matter and other new phenomena in events with an energetic jet and large missing transverse momentum using the ATLAS detector, J. High Energy Phys. 01 (2018) 126, https://doi.org/10.1007/JHEP01(2018)126.

[32] A.M. Sirunyan, et al., Search for dark matter produced with an energetic jet or a hadronically decaying W or Z boson at $\sqrt{s} = 13$ TeV, J. High Energy Phys. 07 (2017) 014, https://doi.org/10.1007/JHEP07(2017)014.

[33] C. Amole, et al., Improved dark matter search results from PICO-2L Run 2, Phys. Rev. D 93 (2016) 061101, https://doi.org/10.1103/PhysRevD.93.061101.

[34] C. Amole, et al., Dark matter search results from the PICO-60 CF_3I bubble chamber, Phys. Rev. D 93 (2016) 052014, https://doi.org/10.1103/PhysRevD.93.052014.

[35] C. Amole, et al., Dark matter search results from the PICO-60 C_3F_8 bubble chamber, Phys. Rev. Lett. 25 (2017) 251301, https://doi.org/10.1103/PhysRevLett.118.251301.

[36] M.G. Aartsen, et al., Improved limits on dark matter annihilation in the sun with the 79-string icecube detector and implications for supersymmetry, J. Cosmol. Astropart. Phys. 04 (2016) 022, https://doi.org/10.1088/1475-7516/2016/04/022.

[37] K. Choi, et al., Search for neutrinos from annihilation of captured low-mass dark matter particles in the Sun by Super-Kamiokande, Phys. Rev. Lett. 114 (2015) 141301, https://doi.org/10.1103/PhysRevLett.114.141301.

[38] M.A. Buckley, Asymmetric dark matter and effective operators, Phys. Rev. D 84 (2011) 043510, https://doi.org/10.1103/PhysRevD.84.043510.